scientific reports

OPEN

Hybridization as a promising approach to engineering the desired performance of bio-nanocomposites: GO-ZnO hybrid reinforced PCL

Parsa Dadashi[2,3], Kosar Torbatinejad[1,3] & Amir Babaei[1✉]

This study investigates the impact of hybridizing graphene oxide (GO) with zinc oxide (ZnO) at varying ratios (1:1 and 1:2) and concentrations (0.5, 0.75, 1 wt%) on the rheological, mechanical, hydrolytic degradation, and antibacterial properties of polycaprolactone (PCL) nanocomposites. GO, ZnO, and GO-ZnO nanohybrids were synthesized and characterized using TEM, AFM, Raman, and FT-IR spectroscopy to confirm their structure and composition. PCL/ZnO nanocomposites were fabricated via solution mixing. Mechanical testing revealed that 0.5 wt% GO-ZnO (1:1) significantly enhanced tensile strength, Young's modulus, and elongation at break, owing to strong interfacial adhesion and uniform dispersion within the PCL matrix. Rheological analysis indicated increased elasticity at 1 wt%, suggesting agglomeration and altered hydrodynamic interactions, while viscosity decreased, particularly at 0.75 wt%, due to sliding effects and accelerated thermal degradation. Hydrolytic degradation tests demonstrated that 0.75 wt% GO-ZnO composites lost 70.2% weight after 26 days in PBS, compared to negligible loss in pure PCL. Antibacterial activity improved by 50% with 0.5 wt% GO-ZnO incorporation. These results underscore PCL/GO-ZnO nanocomposites' enhanced mechanical strength, rapid degradation, and antibacterial efficacy, positioning them as promising candidates for bio-packaging applications.

Global pollution caused by the widespread use of plastics is significantly increasing[1]. As a consequence of necessity of extensive using of polymers, finding degradable alternatives is inevitable[1].

Therefore, a detailed understanding of different classes of biodegradable polymers is crucial. Polyhydroxyalkanoate (PHA), polylactic acid (PLA), polybutylene succinate (PBS), polycaprolactone (PCL), and polysaccharides are biodegradable polymers that can be used as consumable films, and biodegradable packaging instead of using other conventional synthetic packaging materials[2–6]. Among these polymers, PCL, is one of the most useful polymers for agricultural and biomedical applications, exhibiting biocompatibility, biodegradability, and high toughness[3]. The suitable properties of PCL have motivated researchers to investigate the properties of this polymer filled with various nanomaterials as a second component[7]. In a study, microcellular PCL nanocomposites with cellulose nanocrystals (CNCs) showed that higher CNC content in both solid and foamed samples increased tensile modulus, complex viscosities, and storage modulus due to strong reinforcement and interactions between CNCs and PCL[8].

A study compared PCL/clay nanocomposite films made by melt mixing and solvent casting, finding that melt mixing enhanced clay dispersion and mechanical properties due to shear forces. Another study showed that adding graphene to PCL scaffolds improved mechanical properties, with Young's modulus quadrupling at 3 wt% graphene compared to pure PCL. Additionally, PCL/graphene scaffolds with higher graphene content exhibited better biocompatibility, cell adhesion, proliferation, and differentiation when tested with MG-63 osteoblast-like cells, outperforming pure PCL and lower graphene scaffolds[9]. Among the studies focused on the incorporation

[1]Department of Polymer Engineering, Faculty of Engineering, Golestan University, Gorgan 15759-49138, Iran. [2]Advanced Polymer Materials & Processing Lab, School of Chemical Engineering, College of Engineering, University of Tehran, Tehran 14174-66191, Iran. [3]Parsa Dadashi and Kosar Torbatinejad contributed equally to this work. ✉email: a.babaei@gu.ac.ir

of nanomaterials into PCL, zinc oxide (ZnO) nanoparticles and graphene oxide (GO) have attracted significant attention, particularly due to their antibacterial properties and catalytic roles in accelerating degradation[10–13]. These nanoparticles can interestingly aid in controlling the degradation rate of PCL[14,15]. ZnO, a semiconductor with a wide band gap of 3.37 eV and a high excitation binding energy of 60 meV, is classified as a generally recognized safe (GRAS) substance by the Food and Drug Administration and utilized as a food additive[16]. ZnO is extensively used in dermatology, particularly in sunscreens and skincare products. Furthermore, ZnO nanoparticles (NPs) are highly beneficial for wound healing as they promote re-epithelialization, decrease inflammation, and prevent bacterial growth[17–20].

Due to the surface chemistry of ZnO and its unique properties, recent studies have investigated the effects of addition of ZnO hybridized with other nanomaterials on the physical and mechanical properties of polymer nanohybrid composites[21–25]. In a study by De Silva et al., ZnO-coated halloysite (ZnO-Halloysite) was added to PLA films. While films with only ZnO showed weaker mechanical properties than pure PLA, those with ZnO-Halloysite improved tensile strength and modulus. Additionally, these films exhibited strong antibacterial activity, reducing Staphylococcus aureus and Escherichia coli counts by over 99%[26].

A study on PLA/ZnO-TiO$_2$ nanohybrid composites showed that varying nanohybrid content led to excellent dispersion with minimal aggregation in the PLA matrix, enhancing the physical, mechanical, and antibacterial properties of PLA[19].

Among the various ZnO hybridizations with other nanomaterials, investigating the impact of simultaneously blending GO and ZnO hybrids with a polymer matrix is an increasingly promising area of research as a consequence of interesting properties which could bring in by their addition[27]. Few studies explore the performance of polymers with GO-ZnO nanohybrids, highlighting a need for deeper research into their microstructure-property relationships. Our study advances this field by developing GO-ZnO-reinforced PCL nanocomposites for bio-applications, evaluating not only mechanical properties but also rheological, hydrolytic, and antibacterial performance. Unlike prior work, we optimized the GO-to-ZnO ratio in the hybrid filler, revealing how graphene oxide improves dispersion and strength while ZnO enhances antibacterial activity and thermal stability, offering new insights into their combined effects on polymer behavior and degradation kinetics.

Materials and methods

In this study, polycaprolactone (PCL) was used, purchased from Solvay, CAPA 6800 (Belgium), with a density of 1.29 g/cm^3, a melt flow index of 2–4 g/10 min (at 160 °C and 2.16 kg load), and a melting temperature in the range of 58–60 °C. Graphite flakes were obtained from Sigma-Aldrich. Sulfuric acid (H$_2$SO$_4$) with 99% purity, hydrochloric acid (HCl) with 37% purity, and potassium permanganate (KMnO$_4$) were purchased from Arvin Delta Shimi (Iran). Hydrogen peroxide (H$_2$O$_2$) was also sourced from Arvin Delta Shimi (Iran).

Synthesize of GO

The GO nanoparticles used in this study were synthesized using an improved Hummers' method[28]. 3 g of graphite were weighed and mixed with 360 mL of sulfuric acid (H$_2$SO$_4$) and 40 mL of phosphoric acid (H$_3$PO$_4$) in a 9:1 ratio inside an Erlenmeyer flask. The mixture was then stirred on a stirrer for 30–40 min. Next, 18 g of potassium permanganate was slowly added to the flask while maintaining an ice-water bath (at this stage, the solution should turn dark green). The solution was then stirred at 50 °C for 24 h. After 24 h, the solution was cooled to room temperature, and 15 mL of hydrogen peroxide (30% H$_2$O$_2$) and 400 mL of distilled water were added to the flask in an ice bath. After adding H$_2$O$_2$, the solution turned golden, signaling the end of the reaction.

The solution was transferred into Falcon tubes and centrifuged at 4500 rpm for 15 min. The precipitate in the Falcon tubes was then transferred into a Pyrex container and washed three times with 5% hydrochloric acid at 24-h intervals. After 3 days, the solution was placed in a dialysis bag, and the bag was suspended in a container filled with distilled water. The pH of the solution was measured using pH paper. When the pH remained unchanged, the solution was removed from the dialysis bag, and the distilled water in the container was replaced during this period.

Subsequently, the resulting suspension was subjected to ultrasonic treatment for 20 min, followed by a 5-min probe treatment. The suspension was then centrifuged again at 4500 rpm for 5 min to separate the monolayer GO deposited on the Falcon tube. The remaining suspension was subjected to another cycle of ultrasonic and probe treatments. As a result, a stable GO solution with a concentration of 2.52 g/L was obtained. All the processes of synthesizing GO are presented in Fig. 1a.

Synthesize of GO-ZnO nanohybrids

GO-ZnO nanohybrid materials were synthesized in 1:1 and 1:2 weight ratios. The specifications of the materials used in the synthesis of these nanohybrids were reported in Table 1. The GO-ZnO nanohybrid was synthesized using the co-precipitation method. A 0.1 M sodium hydroxide (NaOH) solution and a zinc acetate solution were initially prepared. Solution 1, containing 50 mL of NaOH and 50 mL of distilled water, was then added dropwise to solution 2, containing 33 mL of GO solution and 27 mL of zinc acetate solution, under stirring and ultrasonic treatment (with a 120 W power). This process ensured that the weight ratio of the GO to zinc oxide in the final product was equal. The resulting brown suspension was washed several times with distilled water. The sample was then dried for 24 h using a freeze-drying device. It should be noted that, to reach a precise and specified ratio of GO and ZnO, firstly, ZnO nanoparticles based on the determined amounts of precursors was synthesized and weighed and in the following a given amount of GO was incorporated.

For the GO-ZnO nanohybrid with a 1:2 ratio, solution 2 contained 23 mL of GO and 37 mL of zinc acetate, resulting in a concentration of zinc oxide that was twice that of the GO.
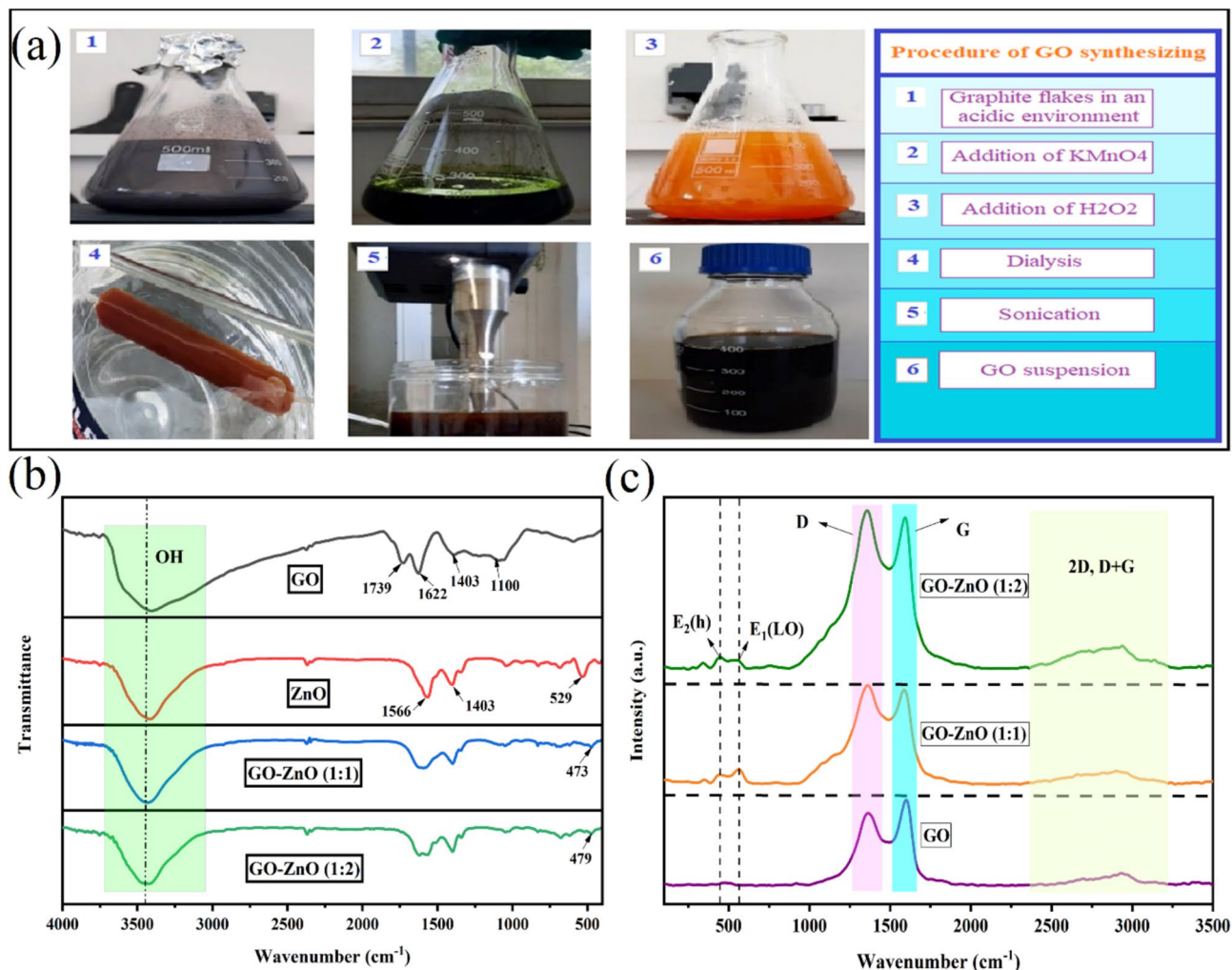
Fig. 1. (**a**) Images illustrating the synthesis of graphene oxide (GO) in this study, (**b**) FT-IR graph for GO, ZnO, GO-ZnO (1:1), and GO-ZnO (1:2) samples, and (**c**) Raman spectroscopy results for GO-ZnO (1:1), GO-ZnO (1:2), and GO samples.

Samples code	PCL (wt%)	GO-ZnO (1:1) (wt%)	GO-ZnO (2:1) (wt%)	ZnO (wt%)
PCL	100	0	0	0
GO-ZnO (1:1) 0.5	99.5	0.5	0	0
GO-ZnO (1:1) 0.75	99.25	0.75	0	0
GO-ZnO (1:1) 1	99	1	0	0
GO-ZnO (1:2) 0.5	99.5	0	0.5	0
GO-ZnO (1:2) 0.75	99.25	0	0.75	0
GO-ZnO (1:2) 1	99	0	1	0
ZnO 0.75	99.25	0	0	0.75

Table 1. Composition of PCL, and nano-hybrids prepared in the study.

Preparation of PCL/GO-ZnO nanocomposites

PCL/GO-ZnO Nanocomposites with 1:1 and 1:2 ratios were fabricated using the solution casting method. The solvent used in this process was dimethylformamide (DMF), purchased from Kimia Aryan Company.

1 g of PCL granules was dissolved in 10 mL of the solvent under magnetic stirring at 50 °C. On the other hand, the desired amount of nanoparticles, measured in grams, was dispersed in 5 mL of the solvent and subjected to an ultrasonic bath for 15 min to separate the GO sheets. The suspension was then probed with 120 W power for 1–2 min to achieve better dispersion of the nanoparticles.

The resulting suspension was then added to the polymer solution and subjected to ultrasonic probing for 1–2 min with 120 W power to achieve a homogeneous suspension. The suspension was then transferred to silicone molds and placed in an oven at 50 °C for 48 h. Due to the sensitivity of GO to high temperatures, all steps were performed under an ice-water bath. Table 1 shows the sample codes and Fig. S1 shows prepared samples.

Characterization

FT-IR spectroscopy

(Fourier Transform Infrared) FT-IR spectroscopy was performed using a Perkin Elmer Spectrum RX1 model to investigate the functional groups in the nanohybrids. For sample preparation and analysis, nanoparticle powders were mixed with KBr to form disks, and the measurements were conducted in the range of 4000–400 cm^{-1}.

Raman analysis

To obtain further confirmation regarding the structure of the GO-ZnO nanohybrid, Raman spectroscopy was employed. The GO and GO-ZnO samples were tested using a TEKSAN 40 Tabān laboratory device, model 1-541N TakRam, with a laser wavelength of 532 nm at room temperature and analyzed accordingly.

Atomic force microscopy (AFM) analysis

GO nanosheets and the GO-ZnO nanohybrid were imaged using an Atomic Force Microscope (AFM) NanoWizard II (JPK, University of Jundi Shapur Ahvaz) in intermittent contact mode. The dimensions of the GO, including its length and thickness, were measured using JPK software.

Transmission electron microscopy (TEM) analysis

The characteristics and morphology of the GO nanoparticle and the GO-ZnO nanohybrid were determined using a TEM. A dilute aqueous solution of the sample was sonicated for 15 min using a sonicator (USA3000, S-Misonix). Then, a drop of the sample was placed onto a perforated carbon film on a 300 mesh copper grid (USA-EMS) and allowed to dry completely at room temperature. The sample was observed with a TEM (C10EM-Zeiss, Carl Zeiss Germany, Kv100) at an accelerating voltage of 100 kV.

Tensile analysis

Tensile or stress–strain testing was conducted to measure the mechanical properties of PCL/GO-ZnO nanocomposites. Tensile strength, elongation at break, and the modulus of the samples, which were 1 cm wide and 7 cm long, were measured at a speed of 10 mm per minute. The device used for this test was the GTECH-3000al model (Taiwan). It is worth noting that five strips were prepared for each sample, and the average results obtained from them were reported.

Rheological analysis

Rheological testing shows the rheological properties (the behavior of polymers in the molten state) of polymer materials. This test was performed on pure PCL samples and their nanocomposites. The rheometer used in this test was the 501MCR model (Paar Anton, Graz, Austria). The testing was conducted at a temperature of 70 °C in an oscillatory mode between two parallel plates, within a frequency range of 0.01–1000 rad/s. The gap between the two plates was 2 mm, and all tests were conducted under a nitrogen atmosphere. Additionally, to obtain results in the linear viscoelastic region, a strain of 1% was applied.

Hydrolytic biodegradability analysis

Hydrolytic degradation of the films was examined in alkaline (NaOH) and neutral phosphate-buffered saline (PBS) solutions. Samples with dimensions of 1×1.5 cm and equal weights were immersed in 10 mL of a 1 M NaOH solution and PBS solution at 50 °C. The weight loss of the samples immersed in the 1 M NaOH solution was monitored over 0–10 days. Every two days, the samples were removed from the solution, washed with distilled water, and dried in an oven at 50 °C for one hour. For the samples in the PBS solution, weight changes were reported over 0–36 days. The weight loss of all samples was calculated using the Eq. (1). In Eq. (1), W_0 is the initial weight, and W_t is the weight of the sample dried at a specific period.

$$Mass\,(\%) = \frac{w_0 - w_t}{w_0} \times 100 \tag{1}$$

Cytotoxicity assay

Cell adhesion and cytotoxicity of PCL and its nanocomposites were evaluated using the MTT assay. Initially, the prepared films were placed in 96-well culture plates, washed three times with PBS, and exposed to UV light for 20 min to sterilize them. The 929L fibroblast cells were cultured in the presence of 10% fetal bovine serum and 1% penicillin/streptomycin. The cells were maintained in a humidified atmosphere at 37 °C with 5% CO$_2$, and the culture medium was replaced every 2 days. When the cells reached over 80% confluence, they were seeded onto the 96-well plates coated with sterilized trypsinized films, as well as on an uncoated plate as a control group. Optical density (OD) at a wavelength of 570 nm was recorded using a Bio-Rad spectrophotometer, and the percentage of cell viability was calculated based on Eq. (2).

$$Survival\ fraction\ = \frac{MeanODintestwells - MeanODincell - freewells}{MeanODincontrolwells - MeanODincell - freewells} \tag{2}$$

X-ray diffraction analysis

XRD analysis was performed using a Siemens D5000 x-ray diffractometer equipped with a copper K-alpha radiation source (wavelength = 0.1540 nm) under ambient conditions. The system featured a rotating anode generator operating at 35 kV and 20 mA. Samples were analyzed in sequential scan mode over a 2θ range of 9°–75°, with diffraction patterns recorded by a scintillation counter detector.

UV–visible analysis

The UV–visible spectrum was recorded using a PG Instruments Ltd UV–Vis spectrophotometer (Model: T90+, UK), scanning wavelengths from 190 to 450 nm, with samples prepared in dilute suspension.

Results and discussion

FT-IR analysis for evaluation of functional groups of synthesized nanoparticles

To study the interaction between GO and ZnO, as well as to verify the formation of the GO-ZnO nanohybrid, FT-IR spectroscopy was used. Figure 1b shows the FT-IR spectra of GO nanoparticles, ZnO, and the GO-ZnO nanohybrid (1:1 and 1:2 ratios) in the range of 400 to 4000 cm^{-1}. In the GO spectrum, characteristic peaks at wavelengths of 1100, 1403, 1622, and 1739 cm^{-1} correspond to the epoxy group (O–C), hydroxyl group, carbon–carbon double bond (C=C), and carbonyl group, respectively[29–31]. In the ZnO spectrum, peaks at 3420 and 1566 cm^{-1} are associated with water molecules within the ZnO nanoparticles, and a peak around 500 cm^{-1} corresponds to the O–Zn bond in ZnO[29,31].

The FT-IR spectrum of the nanohybrids shows that the carbonyl group peak at 1739 cm^{-1} significantly weakens and becomes undetectable, suggesting strong non-covalent interactions, such as hydrogen bonding or coordination between ZnO and the carbonyl groups of GO. A weak O–Zn peak at around 470 cm^{-1} is also observed, confirming the presence of ZnO in the nanohybrids[18]. Notably, the strong peak at 1403 cm^{-1} observed for ZnO is attributed to the adsorption of carbonate (CO_3^{2-}) species on the highly active ZnO surface, which typically occurs upon exposure to atmospheric CO_2. This absorption band overlaps with the C–O stretching vibrations found in GO, leading to a similar appearance in the FTIR spectra. Furthermore, the multiple small peaks observed in the range of 1200–900 cm^{-1} for ZnO are likely due to the adsorbed organic residues originating either from the synthesis process or environmental exposure. For further characterization of GO, refer to the UV–visible spectrum in Fig. S2. This figure reveals a prominent peak at approximately 230 nm, corresponding to π–π* transitions of C=C bonds in sp^2 carbon domains, and a shoulder around 300 nm, attributed to n–π* transitions of C=O bonds in oxygenated functional groups[32–34].

Raman analysis results

Raman spectroscopy was performed to investigate the structure of GO and the GO-ZnO nanohybrid, and the results are reported in Fig. 1c. The characteristic peaks in the Raman spectrum of GO include the D, G, 2D, and G + D peaks at wavelengths of 1362, 1598, 2692, and 2934 cm^{-1}, respectively[18]. The D band is attributed to the carbon vibrations characteristic of defects, indicating structural defects due to the attachment of oxygen-containing functional groups to the basal carbon sheet and other defects arising from severe oxidation. The G band corresponds to in-plane vibrations of the carbon atoms in the sp^2 hybridization state. Also, 2D band represents the multi-layered nature of GO[35,36].

It is well-known that the parameter (I_G/I_D) can be considered to quantify the degree of disorder in a layer structure[18]. This ratio is 0.84 for GO and increased to 1.04 for the case of GO-ZnO hybrid with a 1:1 ratio, and increased further to 1.06 for the 1:2 hybrid. The increase in the (I_G/I_D) ratio from 0.84 (GO) to 1.04 (1:1 GO-ZnO) and 1.06 (1:2 GO-ZnO) demonstrates that the incorporation of ZnO nanoparticles reduces the structural disorder in GO. This trend indicates that ZnO nanoparticles contribute to improving the structural integrity of GO by promoting mild reduction of oxygen functional groups and passivating defect sites. The interaction between ZnO and GO facilitates partial restoration of the sp^2-hybridized carbon network, leading to decreased structural disorder. These findings are consistent with the formation of a more ordered hybrid material as the ZnO content increases.[18,31,37].

Searching the literature, the shift in the location of Raman peaks and changes in the intensity ratio of D/G peak are correlated to the stacking of GO layers during grafting. Accordingly, the changes in the location and intensity ratios of D/G peak of the GO-ZnO compared to the pure GO reveals that ZnO is hybridized with GO sheets.

The blue-shifted Raman peaks and the increased IG/ID ratios in the GO–ZnO nanohybrids suggest the formation of C–O–Zn interactions at oxygen functional groups on GO. These interactions primarily occur at defect sites and help passivate them, thereby preventing further disruption of the sp^2 carbon framework. Simultaneously, a mild reduction of loosely bound oxygen species may occur during the hybridization process, contributing to the partial restoration of the sp^2-hybridized carbon network. These interactions reduce structural disorder, enhance the ordering of the carbon lattice, and improve the overall properties of the material, underscoring the successful synthesis and functional integration of GO and ZnO[31,37]. After hybridization, the domain size of sp^2-hybridized carbon regions in GO becomes smaller, while the number of domains increases. This change can be attributed to the interaction of ZnO nanoparticles with oxygen-containing functional groups at defect sites in GO. These interactions may lead to slight fragmentation of larger sp^2 domains into smaller domains, thereby increasing the number of sp^2 regions while reducing their average size. Furthermore, the hybridization process may restrict the lateral growth of sp^2 domains by passivating defects, ultimately resulting in a more stable, but highly divided, structure. The band observed at a wavelength of 440 cm^{-1} in the GO-ZnO nanohybrid with 1:1 and 1:2 ratios is related to the hexagonal wurtzite crystal phase in zinc oxide. The peak at 573 cm^{-1} is attributed to the formation of a surface defect and vacant sites in O-Zn, corresponding to the optical phonon (LO) of ZnO[18].

The XRD pattern of the GO-ZnO hybrid, presented in Fig. S3, displays distinct diffraction peaks associated with ZnO nanoparticles at 2θ values, corresponding to the (100), (002), and (101) planes of the wurtzite structure, with additional peaks observed up to 40°, consistent with JCPDS card no. 36-1451. These results confirm that the precursor salt (zinc acetate) was successfully reduced and transformed into crystalline ZnO nanoparticles during synthesis. A broad peak at 2θ ≈ 10°–12° is also observed, indicative of the graphene oxide component in the hybrid. The absence of peaks related to the unreacted precursor salt underscores the complete formation of ZnO nanoparticles within the GO-ZnO hybrid.

AFM analysis results

Figure 2a,d shows the AFM image and the height profile of the GO nanosheets. In this image, several GO sheets (with sheet-like morphology) were observed, with a thickness of approximately 1.5 nm and a length of less than or equal to 1 micron. In previous studies, this thickness corresponds to the characteristic value of bilayer GO sheets[18,38]. Figure 2b,e,c,f show the morphology of the synthesized nanohybrids, where the thickness increases from 1.5 nm in GO to about 100 nm in the GO-ZnO nanohybrids. In addition, needle-like zinc oxide nanoparticles formed over the surface of GO nanosheets can be detected[18]. These results are in good agreement with the results from FTIR, and Raman spectroscopy, corroborating the formation of GO-ZnO nanohybrids[18]. According to AFM results, both nanohybrids (1:1) and (1:2) thicknesses are approximately the same and almost near 110 nm.

TEM results

TEM was used to investigate the microstructure and morphology of GO and GO-ZnO nanohybrids, and the obtained images are shown in Fig. 2. Figure 2g shows the morphology of the GO sheets, which are layered and irregular, with some wrinkles on the surface, showing the successful synthesis of mono or two-layered GO. These sheets are large, transparent, and flexible, and they are stacked together with non-covalent bonds. The TEM images of the nanohybrids (Fig. 2h shows that the needle-like ZnO nanoparticles are well-formed on the surfaces of GO. The ZnO nanoparticles are dispersed irregularly within the GO sheets and apparently are in a good interaction and adhesion with them. As shown in Fig. 2h,i, the ZnO nanoparticles in the case of GO-ZnO nanohybrid (1:1) are almost uniform in size and more evenly fabricated and distributed on the surface of GO nanosheets (compare Fig. 2h and Fig. 2i). In other words, a quite more uniform hybrid was synthesized in the case of GO-ZnO (1:1) nanohybrid compared to another counterpart (1:2) (i) It can be said that, in the GO-ZnO nanohybrid (1:2), with the increase in zinc acetate ion concentration, the numbers of zinc ions were increased leading to the higher rate of formation of ZnO nanoparticles[18]. Accordingly, an increase in the size of the ZnO nanoparticles and a decrease in their number was occurred. Nonetheless, lower concentration of zinc ions for the GO-ZnO nanohybrid (1:1) resulted in a more uniformity not only in the size but also in their distribution and consequently a more uniform nanohybrid.

The diameter of the zinc oxide nanoparticles in the GO-ZnO (1:1) hybrid, as estimated by TEM, is about 218 nm, with an average rod length of 508 nm. These values for the (1:2) ratio are 225 nm and 590 nm, respectively[18].

Rheological properties of PCL/GO-ZnO nanocomposites

Rheological testing was performed to investigate the microstructure of PCL/ZnO, PCL/GO-ZnO (1:1), and PCL/GO-ZnO (1:2) nanocomposites in the linear viscoelastic region. Based on this, the rheological properties of all the prepared samples were examined in the linear viscoelastic region to study the dispersion and distribution state and localization of the nanoparticles and consequently, their effect on the microstructure and mechanical performance of prepared samples.

Figure 3a–c show the complex viscosity, storage modulus, and loss modulus as a function of frequency for all fabricated nanocomposites and pure PCL. It is well-known that the complex viscosity of thermoplastic polymers generally exhibits a Newtonian behavior at low frequencies and shear thinning behavior at higher frequencies[39,40]. Pure PCL and its nanocomposites show Newtonian behavior (constant viscosity) at low frequencies and shear thinning at higher frequencies. The storage modulus (G′) of PCL plateaus at low frequencies, reflecting an entanglement network that provides solid-like elasticity in this regime.

Incorporating 0.75 wt% pure ZnO nanoparticles into PCL significantly increased complex viscosity, storage modulus, and loss modulus compared to virgin PCL. Similarly, 0.5 wt% GO-ZnO (1:1) nanohybrid enhanced these properties, though to a lesser extent than ZnO. However, at 0.75 wt% GO-ZnO (1:1), these properties decreased markedly, but they rose again at 1 wt%. This non-monotonic behavior arises from competing effects: GO-ZnO acts as a lubricating agent, reducing viscosity, and as a reinforcing filler, enhancing viscosity through entanglement and interactions with PCL[38]. Additionally, interactions between the GO-ZnO nanohybrids contribute to improved elasticity, while the potential contribution of the nanohybrids in the chain scission process of PCL could also lead to viscosity reduction[18]. Consequently, these competing effects determine the complex rheological behavior observed as the concentration of GO-ZnO nanohybrids is varied. Accordingly, the increase in the complex viscosity observed with the addition of 0.75 wt% ZnO can be attributed to the reduced mobility of the polymer chains as a result of the presence of ZnO nanoparticles[38,41–43]. These nanoparticles hinder the movement of the polymer chains, thereby increasing the viscosity[38]. However, the significant decrease in the complex viscosity upon hybridization of ZnO with GO, at the same concentration of 0.75 wt%, suggests that the effects of GO-ZnO nanohybrid, such as chain scission and lubrication become more dominant[18]. In other words, the presence of GO nanosheets is believed to introduce a lubricating effect, which enhances the overall lubrication and facilitates chain mobility, ultimately reducing viscosity[38]. The increase in the complex viscosity, storage modulus, and loss modulus for samples containing 1 wt% of GO-ZnO (1:1) nanohybrids can be attributed to the formation of a nanohybrids physical network within the PCL matrix. This enhanced elasticity
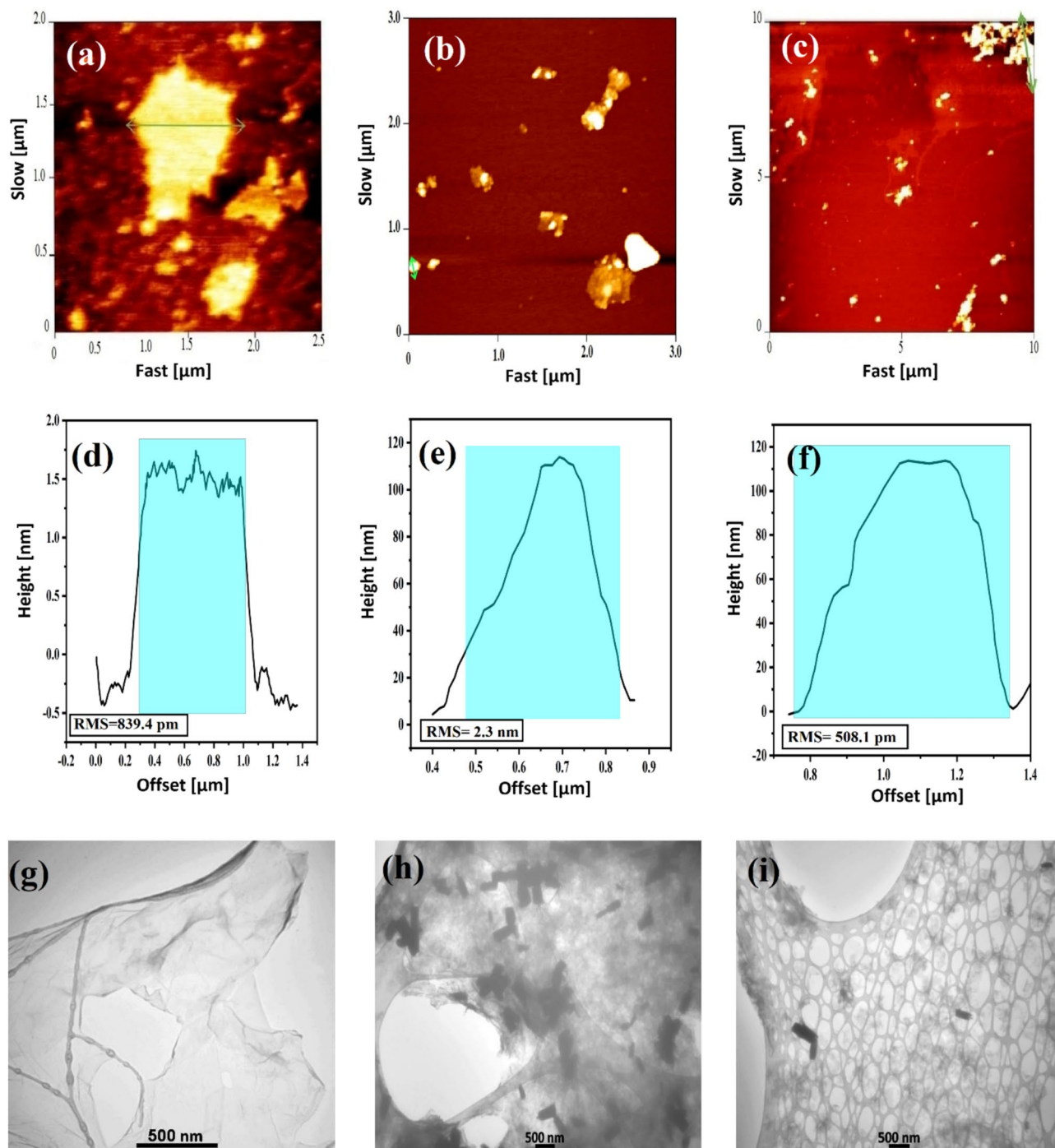
Fig. 2. AFM micrographs of (**a**) GO, (**b**) GO-ZnO (1:1), and (**c**) GO-ZnO (1:2), along with the corresponding height profiles for (**d**) GO, (**e**) GO-ZnO (1:1), and (**f**) GO-ZnO (1:2) samples; and TEM images illustrating (**g**) GO, (**h**) GO-ZnO (1:1), and (**f**) GO-ZnO (1:2) at 500 nm magnifications.

stems from strong interfacial interactions between the GO-ZnO nanohybrids and the PCL matrix, primarily hydrogen bonding between GO's oxygen-containing groups and PCL's carbonyl groups, as well as mechanical reinforcement from dispersed ZnO nanoparticles. These interactions, evidenced by a [e.g., 55%] increase in storage modulus (G') and a [e.g., 12 cm^{-1}] FTIR shift in the C=O peak, dominate over secondary effects such as lubrication or chain scission, driving the observed viscoelastic improvement. Such a same observation has been reported earlier by the other researchers[18].

Figure 3d illustrates the variation of the damping factor (tan δ) with frequency for PCL, PCL/ZnO, and PCL/GO-ZnO samples. It is frequently reported that, the point where tan δ = 1 represents the equilibrium between viscous and elastic behavior, marking the transition from liquid-like to solid-like behavior, or vice versa[43]. As shown in Fig. 3d, introducing 0.75 wt% ZnO resulted in a decrease in the damping factor compared to the virgin
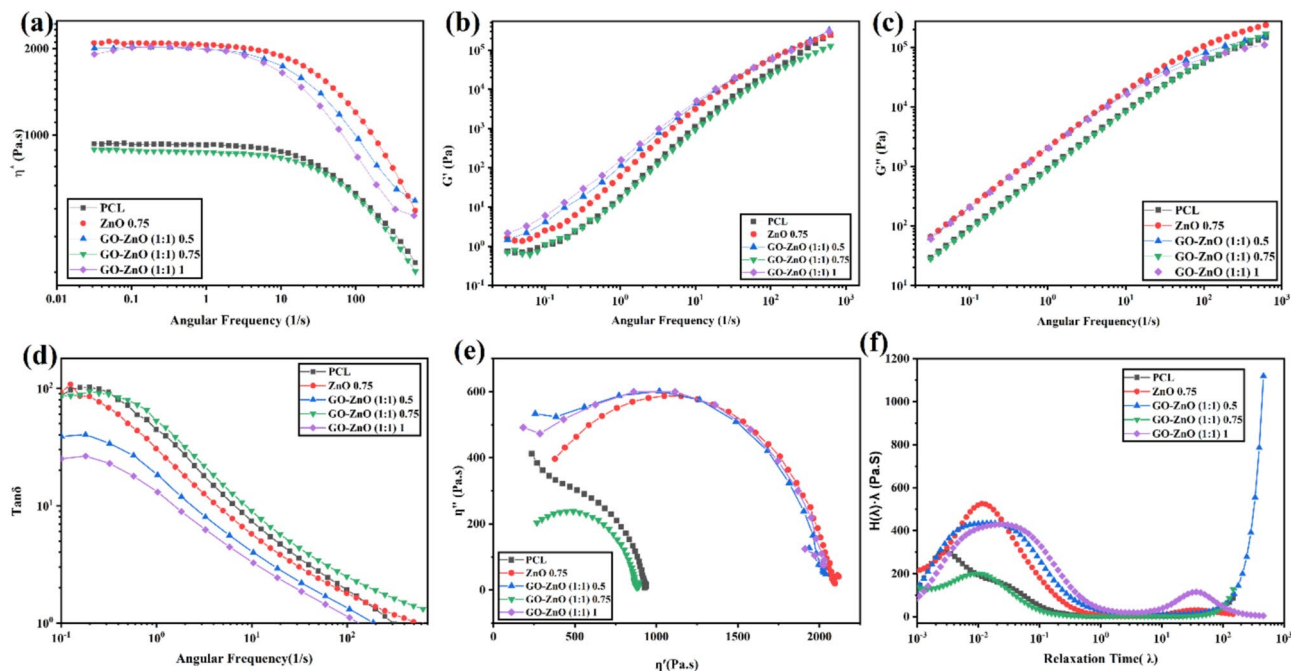
Fig. 3. (**a**) Complex viscosity, (**b**) storage modulus, (**c**) loss modulus, (**d**) damping factor, (**e**) cole–cole, and (**f**) relaxation spectrum plots of PCL, and their nanocomposites with (1:1) ratio.

PCL. Interestingly, adding 0.5 wt% GO-ZnO (1:1) to PCL led to a further reduction in the damping factor. It can be attributed to the lower better dispersion of GO-ZnO nanohybrid, causing less reduction in elasticity due to more engagement of PCL chains and nanohybrids. ZnO is a key factor in decreasing elasticity, primarily through chain scission processes in the polymer. However, when 0.75 wt% GO-ZnO was added to PCL, the damping factor increased, even higher that of virgin PCL. This can be attributed to the dominant lubricating and sliding effects of GO-ZnO as discussed in the previous section. In the following, addition of 1 wt% nanohybrids resulted in a greater reduction in the damping factor compared to other samples, which is another confirmation for the formation of a network structure throughout the material[43].

The Cole–Cole plot is constructed by plotting the loss viscosity ("η) against the real viscosity ('η)[43]. This plot serves as a tool to study the viscoelastic properties of materials with distributed relaxation times[43]. It is also employed to analyze the droplet relaxation phenomenon in polymer blends[44]. However, the Cole–Cole plot alone does not provide sufficient or necessary information about interfacial relaxation, as the interfacial relaxation arc may not fully appear within the experimental frequency range[44].

Changes in the storage modulus relative to the loss modulus are commonly represented by Han plots in Fig. S4, which are widely used to study the microstructure of nanocomposites and the interfacial interactions between the matrix and nanoparticles[41,43,45,46]. These plots are often regarded as a standard tool for evaluating the homogeneity of multi-component systems. A slope of 2 in the terminal region typically signifies a homogeneous system, while deviations from this slope indicate inhomogeneity[47,48]. Additionally, a reduction in slope at low frequencies is often associated with enhanced elasticity[38].

The final slope observed in Han plots is determined by the interplay between hydrodynamic interactions and factors like chain scission or lubrication effects[18]. However, Han plots alone cannot decouple the contributions of these two parameters[18]. In the case of PCL and its nanocomposites, the Han plot slopes remain similar, which suggests that opposing factors affecting elasticity such as the enhancement of hydrodynamic interactions and the reduction due to chain scission and sliding effects counterbalance each other. As a result, the combined effects cannot be distinctly separated in this system[18].

As illustrated in Fig. 3e, the Cole–Cole plots for pure PCL and its nanocomposites reveal a semi-circular arc, indicative of their single-phase and homogeneous structures[43]. As shown, nanocomposites containing 0.5 wt% of both nanohybrids display a larger arc at higher viscosities. It can be corresponded to the good dispersion and distribution of nanohybrids and formation of a physical 3D network of nanohybrids and polymer chains which induce more restriction to polymer chains[47]. These stronger interactions extend the relaxation time, which aligns closely with the observed complex viscosity results.

However, in the nanocomposite containing 0.75 wt% of the nanohybrids, the arc is smaller compared to other samples. This reduction reflects lower elasticity, attributed to the suggestive chain scission of PCL and the lubricating effect introduced by the loaded nanoparticles[41,43]. The ZnO nanoparticles attached to the GO sheets exhibit a catalytic role in polymer chain degradation, which reduces the viscosity of the matrix and facilitates polymer chain movement[43]. Additionally, the sliding effect of GO stacked layers assist in faster relaxation of polymer chains[41].

Interestingly, by the increase of nanohybrids to 1 wt%, the arc noticeably enhanced for both kinds. It can be related to the high amount of added nanoparticles which noticeably restrict the movement of polymer chains and encourage high elasticity to the system and accordingly dominate to the other affecting parameters. It will be discussed more in the next section.

The relaxation spectrum effectively evaluates melt elasticity in multi-component systems, distinguishing relaxation processes. For PCL/GO-ZnO nanocomposites, the relaxation time (λ (H.λ)), shown in Fig. 3f, shifts to higher times compared to pure PCL, indicating nanoparticle-induced restrictions on polymer chain mobility[43]. Additionally, the peak intensity of all nanocomposites were increased, signifying the domination of elastic character of chains[18].

The results demonstrate that, in the case of GO-ZnO (1:1) nanohybrid, when 0.5 wt% is added, a significantly intensified and broad peak of polymer relaxation associated with a long tail at high relaxation times are observed. However, when the nanohybrid loading was increased to 0.75 wt%, a significant reduction in the intensity of both peaks was observed. Very short tail clearly indicates the notable decrease of interaction of polymer and nanoparticles, suggestively as a consequence of inferior dispersion and distribution state of higher amount of nanoparticles. Surprisingly, by addition of 1 wt% of nanohybrid a completely different behavior was observed. A very broad and intensified first peak, a new peak at higher time and disappearance of tail. Such a complex behavior needs a deep analysis to get realized. Typically, the inclusion of nanoparticles is expected to result in primarily elastic behavior within the nanocomposite system, due to interactions with the nanoparticles and consequently slowing the dynamics of polymer chains[43]. However, this study found that introducing nanohybrids to PCL resulted in a primarily viscous behavior. The relaxation spectrum highlights that GO-ZnO nanohybrids can influence the nanocomposites in different ways, depending on their content. indeed, the competition between the factors such as chain scission and reduction in polymer chain molecular weight, the sliding of aggregated nanoparticles, along with other factors that typically enhance elasticity, like polymer-particle and particle–particle interactions, could determine the final behavior of nanocomposites[18]. Multiple parameters influencing nanocomposite performance in opposing ways require differentiation to understand microstructure and property contributions. The relaxation spectrum, a powerful tool, decouples elasticity sources, revealing microstructure details. As shown in Fig. 3f, nanohybrid-loaded samples exhibit broader relaxation spectra than the sharp peak of 0.75 wt% ZnO/PCL, indicating pronounced chain scission by nanohybrids. At 0.5 wt% GO-ZnO (both 1:1 and 1:2 ratios), a spectrum tail reflects strong PCL-nanohybrid interfacial interactions and good dispersion. Additionally, GO-ZnO (1:1) shows a second relaxation peak, suggesting confined polymer chains in nanohybrid 3D networks at high relaxation times[49].

Figure 4 exhibits the results of the rheological test for the nanocomposites incorporating a second type of nano-hybrid (GO-ZnO (1:2)). Generally, a same trend regarding the rheological behavior as a consequence of loaded nanohybrid was observed which was extensively discussed above. However, we need to compare the nanocomposites at identical added nanofillers to investigate the effect of different conditions of nanohybrids on the final performance of nanocomposites.

Figure 5 represents a rheological comparison between GO-ZnO (1:1) and GO-ZnO (1:2) at two concentrations (0.5 wt% and 0.75 wt%), and pure PCL. As shown in Fig. 5, the GO-ZnO (1:1) hybrids exhibited
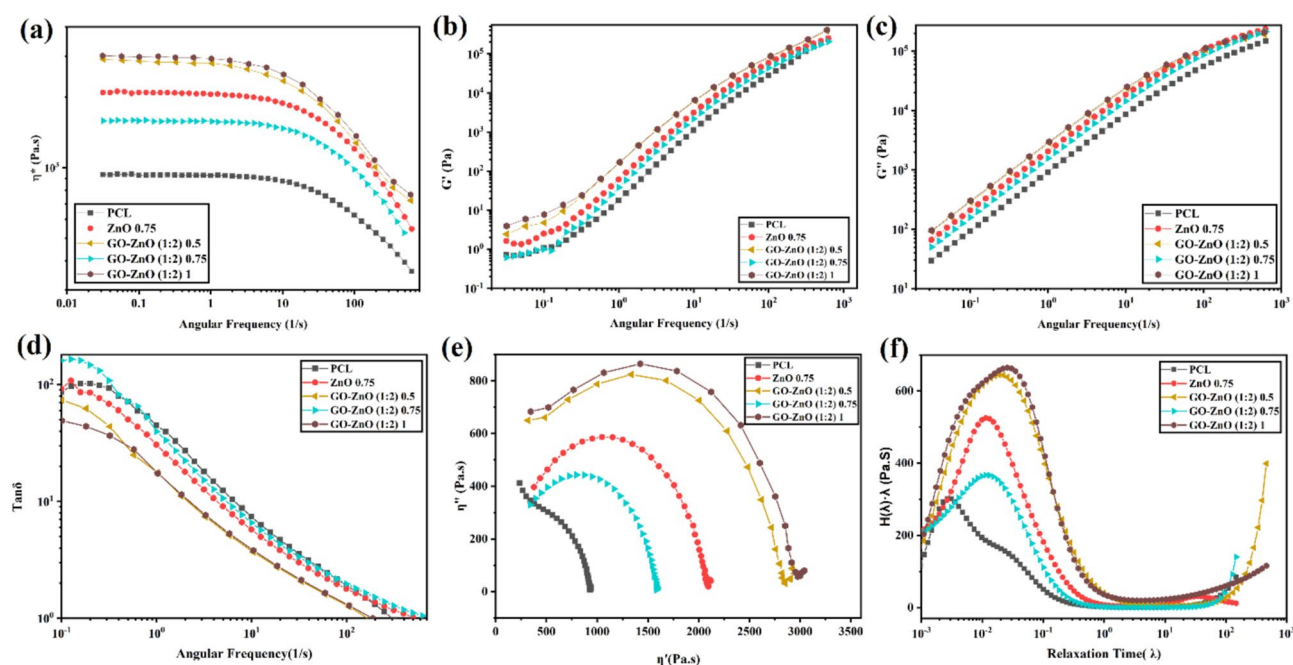
Fig. 4. (**a**) Complex viscosity, (**b**) storage modulus, (**c**) loss modulus, damping factor, cole–cole, and relaxation spectrum plots of PCL, and their nanocomposites with (1:2) ratio.
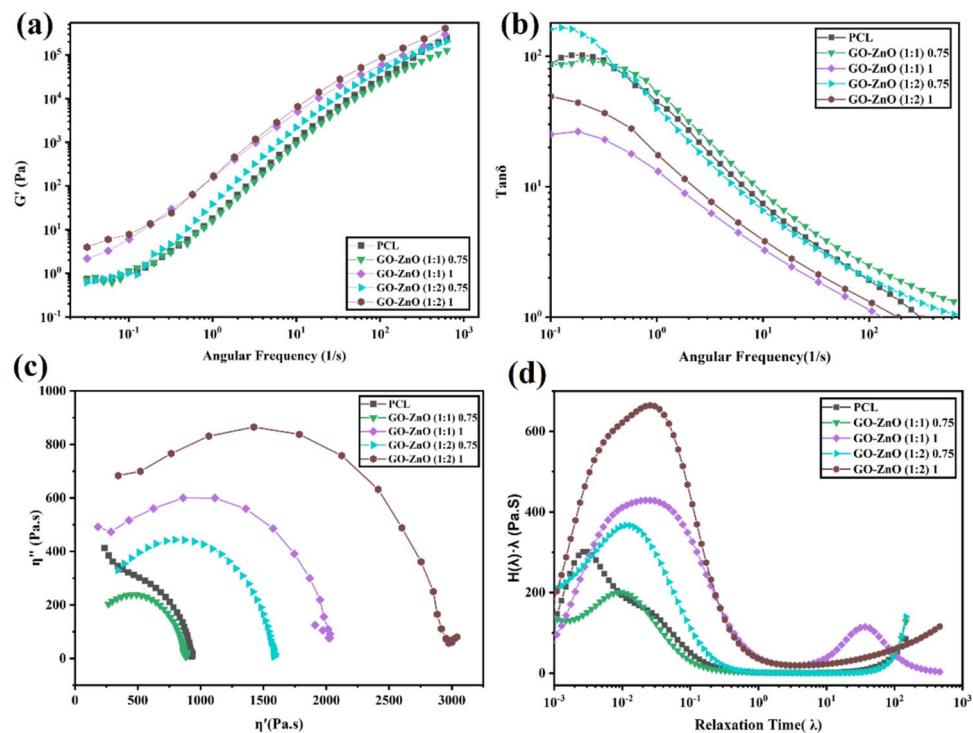
Fig. 5. Comparison of rheological properties between the ratio of GO-ZnO (1:1) and GO-ZnO (1:2) nanohybrids.

Sample	Tensile strength (MPa)	Young modulus (MPa)	Elongation at break (%)
PCL	17.7 ± 0.7	235.1 ± 7.4	623.8 ± 7.4
GO-ZnO (1:1) 0.5	22.7 ± 3.2	340.1 ± 6.2	1011.9 ± 20.8
GO-ZnO (1:1) 0.75	20.3 ± 0.9	330.1 ± 51.4	515.2 ± 15.2
GO-ZnO (1:1) 1	16.8 ± 0.4	325.3 ± 7.5	342.3 ± 17.3
GO-ZnO (1:2) 0.5	15.3 ± 0.6	263.4 ± 8.6	267.4 ± 26.1
GO-ZnO (1:2) 0.75	15.2 ± 0.5	262.4 ± 28.6	260.1 ± 35.2
GO-ZnO (1:2) 1	15.2 ± 0.7	261.3 ± 36.2	252.4 ± 15.7
ZnO 0.75	19.5 ± 4.2	320.3 ± 27.8	510.1 ± 40.3

Table 2. Mechanical Properties of PCL and their Nanocomposite Samples Containing ZnO and GO-ZnO Nano-hybrid.

a greater reduction in storage modulus compared to GO-ZnO (1:2) at both concentrations. Additionally, the loss tangent increased more noticeably, the Cole–Cole diagram diameter expanded greater, and The intensity of the relaxation spectrum increased and shifted to the right, indicating higher elasticity in the (1:2) ratio samples compared to the (1:1) ratio. A similar trend was observed for the 1 wt% sample; however, it is not included in the graph as its representation would be difficult to discern.

This behavior is attributed to the well-hybridized structure and finer nanohybrid morphology of GO-ZnO (1:1), as supported by AFM/TEM analysis of the synthesized nanohybrids. The improved degradation and lubrication effects of GO-ZnO (1:1) reduced the elasticity of nanocomposites greater relative to GO-ZnO (1:2). The lower viscosity of GO-ZnO (1:1), which indicates easier processing, suggests that this sample is the most promising candidate for packaging applications.

Mechanical properties of PCL/GO-ZnO nanocomposites

To study the effect of adding ZnO nanoparticles and GO-ZnO nanohybrids on the mechanical performance of PCL, a tensile test was conducted on the nanocomposites and pure PCL, and the results are reported in Table 2. As a case study stress–strain curve of PCL sample can be observed in Fig. S5.

The incorporation of 0.5 wt% GO-ZnO (1:1) nanohybrid significantly enhanced the tensile strength, modulus, and elongation at break by 28%, 44%, and 62%, respectively, compared to unreinforced PCL. This improvement can be attributed to the uniform dispersion of the GO-ZnO (1:1) nanohybrid and its strong interfacial bonding with the PCL matrix[38]. TEM images of GO-ZnO (1:1) nanohybrids, shown in Fig. S6 of the

supplementary information, reveal excellent dispersion within the PCL matrix, supporting this interpretation. The high surface area of graphene oxide (GO) facilitates effective load transfer, while ZnO nanoparticles enhance matrix reinforcement through favorable interactions with PCL chains. These interactions promote uniform stress distribution, reducing stress concentration sites and enabling higher elongation at break[18]. However, increasing the nanohybrid content to 0.75 wt% and 1 wt% led to a decline in tensile properties, with 1 wt% samples exhibiting tensile strength and elongation at break below those of pure PCL. This decrease is primarily due to nanohybrid agglomeration at higher loadings, which restricts PCL chain mobility and introduces stress concentration points, promoting premature fracture[38].

In contrast, PCL/GO-ZnO (1:2) nanocomposites displayed a consistent decrease in tensile strength and elongation at break across all loadings, with only a modest 12% increase in modulus. The higher ZnO content in the 1:2 ratio results in larger nanoparticle aggregates, as observed in prior dispersion analyses, which act as stress concentration sites[38]. These aggregates disrupt load transfer and weaken the composite, reducing tensile strength and ductility. The slight modulus increase reflects the inherent stiffness of GO (theoretical modulus ~ 1000 GPa), which partially compensates for the poor dispersion.

To elucidate the role of individual components, a nanocomposite with 0.75 wt% pure ZnO was prepared and compared to those with GO-ZnO nanohybrids at the same loading. The ZnO-only nanocomposite exhibited a 10% increase in tensile strength and a 36% increase in modulus compared to pure PCL, indicating moderate reinforcement. In contrast, the 0.75 wt% GO-ZnO (1:1) nanohybrid outperformed the ZnO-only sample, highlighting the synergistic effect of GO-ZnO hybridization in enhancing load transfer and matrix interaction. However, the 0.75 wt% GO-ZnO (1:2) nanocomposite showed inferior tensile strength compared to both the 1:1 and ZnO-only samples, underscoring the detrimental effect of excess ZnO-induced agglomeration[18].

Hydrolytic degradation analysis of PCL/GO-ZnO nanocomposites

One of the most promising applications of PCL is use as biodegradable products[42,43,50,51]. Therefore, gaining a deep understanding about the degradation mechanisms or the methods to facilitate or control the rate of degradation can lead us to use them in an engineered path. The literature survey shows that, the most significant factor in the degradation of PCL is hydrolysis[42,43,50,51]. It is generally accepted that the degradation of PCL is due to the hydrolytic cleavage of ester bonds[43]. When the bonds in the polymer chains react with water molecules, the chain length of the degraded polymers is reduced[43]. The end groups in the small chain fragments are carboxylic acids, which render the polymer soluble in water[43]. This mechanism is based on the equilibrium between hydronium (H^+) and hydroxyl (OH^-) ions in the environment[43]. At a pH of 7, this equilibrium is neutral, and hydrolysis occurs over a prolonged period[43].

Previous studies have reported that for physiological applications, PCL film at 37 °C (body temperature) takes approximately 30 days to reduce its molecular weight from 30 to 21 kDa, and about 60 days to reach 20 kDa[43]. The degradation process can be accelerated in two ways: by increasing temperature or altering pH. Accelerated degradation by temperature, according to the ASTM 1980-02F standard, assumes the Arrhenius rate function, where a 10 °C increase in temperature (to approximately 47 °C) doubles the degradation rate[43].

The pH of environment strongly influences the hydrolysis of PCL and can occur in either acidic or basic conditions. Unlike acid-catalyzed hydrolysis, which is reversible, base-catalyzed hydrolysis is irreversible because the reaction proceeds to complete in the final step, converting carboxylic acid to the carboxylate ion[43].

In this study, we first investigated the effect of temperature on the rate of degradation of fabricated samples, using PBS solution (pH 7.4) at 50 °C and subsequently examined the effects of both temperature and pH using 1 M sodium hydroxide (NaOH) at 50 °C. The obtained results are shown in Table 4.

According to Table 3, pure PCL did not degrade over the 36-day test period, which can be attributed to its tough and hydrophobic nature. Also, in all nanocomposites, no degradation or weight loss was observed during the 0–16 day period. In the following, it was observed that all samples transitioned from a tough to brittle state initially, and the weight loss began after 16 days. Table 3 illustrates the physical degradation of the films after 36 days. It can be observed that, the addition of nanoparticles increased the polymer degradation rate noticeably. This can be explained by the increased interfacial area between nanohybrids and PCL, which accelerates the hydrolysis rate. Additionally, it can be observed that more weight loss occurs in case of nanocomposites having 0.75 wt% of GO-ZnO (1:2) compared to 0.75 wt% ZnO alone. This illustrates that the hybridization of GO and ZnO can help improve the rate of hydrolytic degradation because the synergistic interaction between GO and ZnO enhances the dispersion and catalytic activity of ZnO nanoparticles, providing more active sites for

Sample name	Mass loss (wt.%) (0–16 days)	Mass loss (wt.%) (16–26 days)	Mass loss (wt.%) (26–32 days)
PCL	0	0	0
GO-ZnO (1:1) 0.5	0	0	2.7
GO-ZnO (1:1) 0.75	0	18.6	21.6
GO-ZnO (1:1) 1	0	66	75
GO-ZnO (1:2) 0.5	0	0	11.9
GO-ZnO (1:2) 0.75	0	70.2	80.8
GO-ZnO (1:2) 1	0	78	85.4
ZnO 0.75	0	35	80

Table 3. Degradation rate of PCL and its nanocomposites in PBS at 50 °C.

hydrolysis[18]. Additionally, it can be observed that GO-ZnO nanohybrids with a 1:2 ratio exhibit greater hydrolytic degradation activity compared to those with a 1:1 ratio, which can be attributed to the more significant role of ZnO in hydrolytic degradation relative to GO[18].

Generally, the rate of hydrolysis of polyesters in the presence of nanoparticles depends on the various factors, such as the morphology of the nanoparticles, their dispersion, and their hydrophilicity or hydrophobicity[14,42,52,53]. The nanocomposite containing GO-ZnO (1:2) nanohybrid showed a faster degradation and weight loss compared to the nanocomposite containing the GO-ZnO (1:1) nanohybrid[18]. Specifically, the (1:2) nanocomposites behaved more brittle and fragile after 16 days in PBS solution. This behavior can be ascribed to the destructive role of ZnO in association with the specific morphology and size of ZnO in hybrid and also the dispersion state of them[18]. ZnO nanoparticles act as a catalyst for the degradation of aliphatic polyesters, breaking ester bonds and increasing the hydrolysis rate[18]. The higher concentration and larger size of ZnO nanoparticles along with the inferior quality of dispersion in the GO-ZnO (1:2) nanohybrid are the factors that accelerate the rate of degradation more than the counterpart one.

Figure 6 shows the weight loss of PCL, PCL/ZnO and PCL/GO-ZnO nanocomposites in the environment of 1 M of NaOH. As can be observed, with the increase of pH as a factor, the degradation process accelerated. Pure PCL film degraded within 240 h, and by increase in the percentage of nanohybrids a rise in the degradation rate of the nanocomposites was observed. In samples containing 1 wt% of both GO-ZnO nanohybrids, the weight loss rate was higher compared to the other samples (0.5 and 0.75 wt%) which was expectable because of higher amount of loaded nanohybrids.

Additionally, in Fig. 6, the samples containing 0.75 wt% ZnO and 1 wt% GO-ZnO (1:1) hybrid showed a similar degradation trend, suggesting that hybridizing GO and ZnO slightly reduced the degradation rate compared to the nanocomposite containing only ZnO[18]. This can be attributed to lower amount of ZnO present in the hybrid and also suggestive the sheet-like morphology of GO. Meaning that, the flat GO sheets make it more difficult for the solution to reach the polymer chains[18]. As with the degradation trend in PBS, the nanocomposites containing GO-ZnO (1:2) nanohybrids degraded faster than those containing GO-ZnO (1:1) nanohybrids (Fig. S7). The PCL/GO-ZnO (1:1) 1% nanocomposite degraded in 168 h, while its counterpart degraded in 144 h.

Biocompatibility analysis of PCL/GO-ZnO nanocomposites

The *biocompatibility* term is a general concept referring to a material's compatibility with living tissue[54]. A more useful definition of biocompatibility is the ability of a material to elicit an appropriate response in the presence of a host for a specific application[54]. An appropriate host response requires identifying and characterizing tissue reactions and responses.

The cytotoxicity test (MTT) is one of the methods to study the toxicity of materials on cells in vitro[54]. For all nanocomposites and pure PCL, MTT assays were conducted and the results are shown in Table 4. Table 4 shows
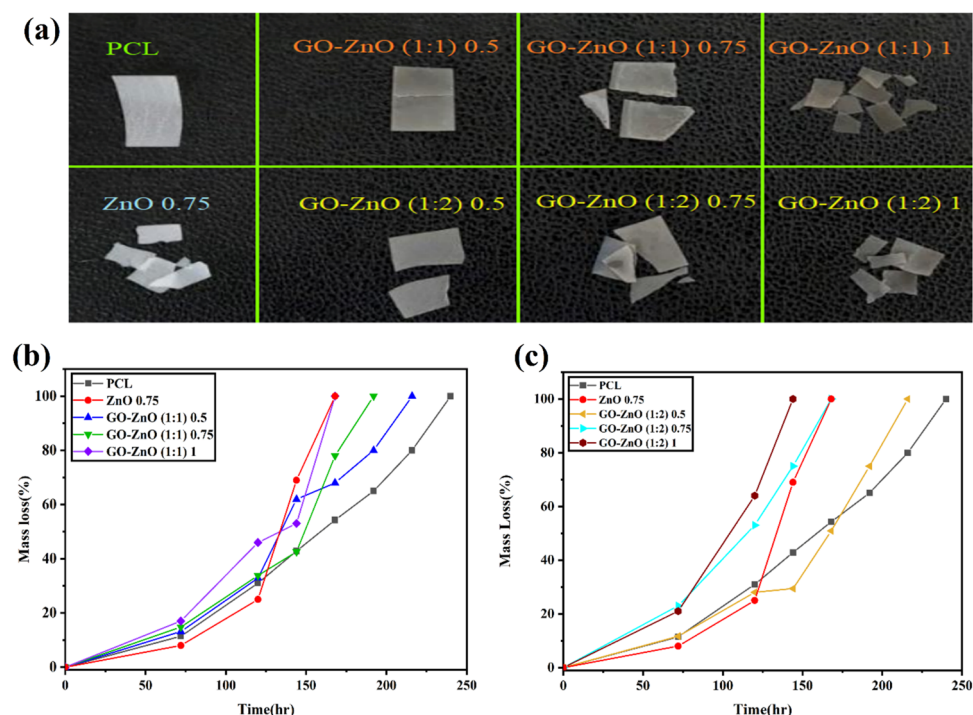
Fig. 6. (**a**) Illustration of samples after hydrolytic degradation after 36 days, plots of Mass Loss (%) versus Time (hr) for PCL, (**b**) GO-ZnO (1:1), and (**c**) GO-ZnO (1:2) nano-hybrids in 1M of NaOH at 50 °C.

Sample name	Cell viability (%)	Stdev (± %)
PCL	100	2
GO-ZnO (1:1) 0.5	96	2.5
GO-ZnO (1:1) 0.75	95	2.8
GO-ZnO (1:1) 1	94	3
GO-ZnO (1:2) 0.5	48	4.5
GO-ZnO (1:2) 0.75	47	3.8
GO-ZnO (1:2) 1	46	2
ZnO 0.75	100	3.2

Table 4. Cell viability (%) for PCL and its nanocomposites containing GO-ZnO nano-hybrids with different ratios of GO to ZnO (1:1) and (2:1).

that samples of PCL, PCL/ZnO, and PCL/GO-ZnO (1:1) nanocomposites exhibited more than 90% cell viability, making them suitable for biomedical applications.

One factor influencing nanocomposites' cytotoxicity is ZnO nanoparticles, which can release Zn^{2+} ions into cells[54]. Incorporating ZnO nanoparticles into the polymer matrix helps to control the release of Zn^{2+} ions, making the films safer for use[54]. Another cytotoxic effect of ZnO is its ability to generate reactive oxygen species (ROS), which can alter mitochondrial membrane potential, cause lysosomal instability, damage DNA, and lead to cell death[54]. However, the release level of ZnO in nanocomposites is more than three times lower than the concentration of ZnO nanoparticles, making the nanocomposites safe for medical and packaging applications[54]. The point should be noted is that, nanohybridization increases the cytotoxicity which can be correlated to the combination of sharp edges of GO and biocidal nature of ZnO. However, this increase was not notable in the case of GO-ZnO (1:1) nanohybrid, probably due to the specific kind of morphology and better dispersion state of this nanohybrid. Furthermore, it can be clearly observed that, PCL/GO-ZnO (1:2) nanocomposites showed significantly higher cytotoxicity compared to the other counterparts. Such results can be attributed to the combination of sharp edges of GO, ROS generation, and higher zinc acetate ion concentration arising from the higher amount and bigger size of ZnO in the hybrid as well as inferior dispersion of them[54].

Finally, what sets this study apart is our deep dive into the synergistic reinforcement effect of GO-ZnO within the PCL matrix, revealing how this hybrid filler enhances structural integrity, modulates viscosity for improved processability, and accelerates hydrolytic degradation for controlled biodegradability. Beyond mechanical improvements, we explore the critical role of GO-ZnO in imparting exceptional antibacterial activity, positioning our nanocomposite as an ideal candidate for biomedical implants, tissue engineering scaffolds, and antibacterial packaging. This work is not just an incremental advancement but a breakthrough in designing high-performance, sustainable biomaterials with precisely engineered rheological behavior, enhanced durability, and bio-functionality. By leveraging advanced nanohybrid synthesis, tailored dispersion techniques, and multi-scale property assessments, we bridge the gap between material innovation and real-world bio-applications, marking a significant milestone in the evolution of biodegradable polymer nanocomposites.

Conclusion

This study demonstrated that GO-ZnO nanohybrids enhance PCL nanocomposites for bio-packaging. At 0.5 wt% GO-ZnO (1:1), tensile strength, modulus, and elongation increased by 28%, 44%, and 62%, respectively, due to uniform dispersion and strong interfacial bonding, though higher loadings reduced performance via agglomeration. Rheological analysis showed non-monotonic elasticity, balancing reinforcement and chain sliding. The 0.75 wt% GO-ZnO (1:2) accelerated degradation (70% weight loss in 26 days), driven by ZnO's catalytic effect and GO's active sites. Antibacterial activity (50% bacterial reduction) and high cell viability (> 90% for 1:1) highlight their potential. Optimized nanohybrid ratios could further advance sustainable biodegradable materials.

References

1. Flury, M. & Narayan, R. Biodegradable plastic as an integral part of the solution to plastic waste pollution of the environment. *Curr. Opin. Green Sustain. Chem.* **30**, 100490 (2021).
2. Ebrahimi, F. & Ramezani Dana, H. Poly lactic acid (PLA) polymers: from properties to biomedical applications. *Int. J. Polym. Mater. Polym. Biomater.* **71**, 1117–1130 (2022).
3. Malikmammadov, E., Tanir, T. E., Kiziltay, A., Hasirci, V. & Hasirci, N. PCL and PCL-based materials in biomedical applications. *J. Biomater. Sci. Polym. Ed.* **29**, 863–893 (2018).
4. Aravamudhan, A., Ramos, D. M., Nada, A. A. & Kumbar, S. G. Natural polymers: polysaccharides and their derivatives for biomedical applications. In *Natural and Synthetic Biomedical Polymers* 67–89 (Elsevier, 2014).
5. Keskin, G., Kızıl, G., Bechelany, M., Pochat-Bohatier, C. & Öner, M. Potential of polyhydroxyalkanoate (PHA) polymers family as substitutes of petroleum based polymers for packaging applications and solutions brought by their composites to form barrier materials. *Pure Appl. Chem.* **89**, 1841–1848 (2017).
6. Barletta, M. et al. Poly (butylene succinate)(PBS): Materials, processing, and industrial applications. *Prog. Polym. Sci.* **132**, 101579 (2022).

7. Luduena, L. N., Alvarez, V. A. & Vazquez, A. Processing and microstructure of PCL/clay nanocomposites. *Mater. Sci. Eng. A* **460**, 121–129 (2007).

8. Mi, H.-Y. et al. Poly (ε-caprolactone)(PCL)/cellulose nano-crystal (CNC) nanocomposites and foams. *Cellulose* **21**, 2727–2741 (2014).

9. Anitasari, S., Wu, C.-Z. & Shen, Y.-K. PCL/graphene scaffolds for the osteogenesis process. *Bioengineering* **10**, 305 (2023).

10. Dreyer, D. R., Park, S., Bielawski, C. W. & Ruoff, R. S. The chemistry of graphene oxide. *Chem. Soc. Rev.* **39**, 228–240 (2010).

11. Seabra, A. B., Paula, A. J., de Lima, R., Alves, O. L. & Durán, N. Nanotoxicity of graphene and graphene oxide. *Chem. Res. Toxicol.* **27**, 159–168 (2014).

12. Kołodziejczak-Radzimska, A. & Jesionowski, T. Zinc oxide—from synthesis to application: a review. *Materials (Basel).* **7**, 2833–2881 (2014).

13. Wöll, C. The chemistry and physics of zinc oxide surfaces. *Prog. Surf. Sci.* **82**, 55–120 (2007).

14. Sánchez-González, S., Diban, N. & Urtiaga, A. Hydrolytic degradation and mechanical stability of poly (ε-Caprolactone)/reduced graphene oxide membranes as scaffolds for in vitro neural tissue regeneration. *Membranes (Basel).* **8**, 12 (2018).

15. Felice, B. et al. Controlled degradability of PCL-ZnO nanofibrous scaffolds for bone tissue engineering and their antibacterial activity. *Mater. Sci. Eng. C* **93**, 724–738 (2018).

16. Javed, R., Usman, M., Tabassum, S. & Zia, M. Effect of capping agents: structural, optical and biological properties of ZnO nanoparticles. *Appl. Surf. Sci.* **386**, 319–326 (2016).

17. Martin, M., Prasad, N., Sivalingam, M. M., Sastikumar, D. & Karthikeyan, B. Optical, phonon properties of ZnO–PVA, ZnO–GO–PVA nanocomposite free standing polymer films for UV sensing. *J. Mater. Sci. Mater. Electron.* **29**, 365–373 (2018).

18. Khaleghi, R., Dadashi, P. & Babaei, A. Investigating the effect of GO-ZnO nano-hybrid on the mechanical, rheological, and degradation performance of poly (butylene succinate). *Polym. Compos.*

19. Tajdari, A., Babaei, A., Goudarzi, A. & Partovi, R. Preparation and study on the optical, mechanical, and antibacterial properties of polylactic acid/ZnO/TiO$_2$ shared nanocomposites. *J. Plast. Film Sheet.* **36**, 285–311 (2020).

20. Mahdavi, H., Kerachian, M. A. & Abazari, M. Synergistic effect of GO@ SiO$_2$ and GO@ ZnO nano-hybrid particles with PVDF-g-PMMA copolymer in high-flux ultrafiltration membrane for oily wastewater treatment and antifouling properties. *J. Ind. Eng. Chem.* **108**, 374–388 (2022).

21. Zabihi, E. et al. Facile and rapid in-situ synthesis of chitosan-ZnO nano-hybrids applicable in medical purposes; a novel combination of biomineralization, ultrasound, and bio-safe morphology-conducting agent. *Int. J. Biol. Macromol.* **131**, 107–116 (2019).

22. Padinhattayil, S. & Rai, K. S. PVA/GO-ZnO hybrid nanocomposites: Synthesis. *Anal. Appl. Indian J. Sci. Technol.* **14**, 1982–1992 (2021).

23. Xu, T., Zhang, L., Cheng, H. & Zhu, Y. Significantly enhanced photocatalytic performance of ZnO via graphene hybridization and the mechanism study. *Appl. Catal. B Environ.* **101**, 382–387 (2011).

24. Giannakas, A. E. et al. Nanocomposite film development based on chitosan/polyvinyl alcohol using ZnO@ montmorillonite and ZnO@ halloysite hybrid nanostructures for active food packaging applications. *Nanomaterials* **12**, 1843 (2022).

25. Paraschiv, C., Hristea, G., Iordoc, M., Sbarcea, B. G. & Marinescu, V. Hydrothermal growth of ZnO/GO hybrid as an efficient electrode material for supercapacitor applications. *Scr. Mater.* **195**, 113708 (2021).

26. De Silva, R. T., Pasbakhsh, P., Lee, S. M. & Kit, A. Y. ZnO deposited/encapsulated halloysite–poly (lactic acid)(PLA) nanocomposites for high performance packaging films with improved mechanical and antimicrobial properties. *Appl. Clay Sci.* **111**, 10–20 (2015).

27. Víctor-Román, S. et al. Controlling the surface chemistry of graphene oxide: Key towards efficient ZnO-GO photocatalysts. *Catal. Today* **357**, 350–360 (2020).

28. Zaaba, N. I. et al. Synthesis of graphene oxide using modified hummers method: solvent influence. *Proc. Eng.* **184**, 469–477 (2017).

29. Puneetha, J., Kottam, N. & Rathna, A. Investigation of photocatalytic degradation of crystal violet and its correlation with bandgap in ZnO and ZnO/GO nanohybrid. *Inorg. Chem. Commun.* **125**, 108460 (2021).

30. Kafashan, A. & Babaei, A. Development and investigation of a polysaccharide ternary nanocomposite based on basil seed gum/graphene oxide/anthocyanin for intelligent food packaging. *Int. J. Biol. Macromol.* **280**, 135537 (2024).

31. Azizpour, N. et al. Films of polylactic acid with graphene oxide-zinc oxide hybrid and *Mentha longifolia* essential oil: Effects on quality of refrigerated chicken fillet. *Int. J. Food Microbiol.* **426**, 110893 (2025).

32. Chowdhury, I., Duch, M. C., Mansukhani, N. D., Hersam, M. C. & Bouchard, D. Interactions of graphene oxide nanomaterials with natural organic matter and metal oxide surfaces. *Environ. Sci. Technol.* **48**, 9382–9390 (2014).

33. Marcano, D. C. et al. Improved synthesis of graphene oxide. *ACS Nano* **4**, 4806–4814 (2010).

34. Tang, Q.-L. & Luo, Q.-H. Adsorption of CO$_2$ at ZnO: a surface structure effect from DFT+ U calculations. *J. Phys. Chem. C* **117**, 22954–22966 (2013).

35. Kafashan, A., Joze-Majidi, H., Kazemi-Pasarvi, S., Babaei, A. & Jafari, S. M. Nanocomposites of soluble soybean polysaccharides with grape skin anthocyanins and graphene oxide as an efficient halochromic smart packaging. *Sustain. Mater. Technol.* **38**, e00755 (2023).

36. Arefkhani, M., Babaei, A., Masoudi, M. & Kafashan, A. A step forward to overcome the cytotoxicity of graphene oxide through decoration with tragacanth gum polysaccharide. *Int. J. Biol. Macromol.* **226**, 1411–1425 (2023).

37. Dehghan, F., Dadashi, P., Babaei, A. & Partovi, R. Biodegradable PLA films incorporating GO-ZnO hybrid and *Mentha longifolia* oil: Fabrication and characterization. *Polym. Eng. Sci.*

38. Dadashi, P., Babaei, A. & Khoshnood, M. Investigating the role of PA6/GO interactions on the morphological, rheological, and mechanical properties of PA6/ABS/GO nanocomposites. *Polym. Technol. Mater.* 1–15 (2022).

39. Krishnamoorti, R., Banik, I. & Xu, L. Rheology and processing of polymer nanocomposites. *Rev. Chem. Eng.* **26**, 3–12 (2010).

40. Newman, J. K. Dynamic shear rheological properties of polymer-modified asphalt binders. *J. Elastomers Plast.* **30**, 245–263 (1998).

41. Sadri, S. A., Arefkhani, M., Dadashi, P., Babaei, A. & Abbasi. Investigating compatibilization of polyoxymethylene/styrene-butadiene-styrene immiscible blend through addition of hydroxylated graphene. *Sci. Rep.* **14**, 24734 (2024).

42. Dadashi, P., Babaei, A. & Abdolrasouli, M. H. Investigating the hydrolytic degradation of PLA/PCL/ZnO nanocomposites by using viscoelastic models. *Polym. Eng. Sci.* **62**, 869–882 (2022).

43. Ahmadzadeh, Y., Babaei, A. & Goudarzi, A. Assessment of localization and degradation of ZnO nano-particles in the PLA/PCL biocompatible blend through a comprehensive rheological characterization. *Polym. Degrad. Stab.* **158**, 136–147 (2018).

44. Elhamnia, M., Motlagh, G. H. & Jafari, S. H. A multiple approach in determination of interfacial tension of biodegradable melt-mixed PBAT/EVOH blends: Correlation of morphology, rheology and mechanical properties. *Polym. Test.* **82**, 106301 (2020).

45. Dadashi, P., Babaei, A. & Khoshnood, M. Investigating the role of PA6/GO interactions on the morphological, rheological, and mechanical properties of PA6/ABS/GO nanocomposites. *Polym. Technol. Mater.* **62**, 756–770 (2023).

46. Dadashi, P., Ray, S. S. & Babaei, A. Effect of graphene oxide localization on morphology development and rheological and mechanical properties of poly(lactic acid)/ethylene vinyl alcohol copolymer blend composites: a comprehensive study. *Polymers (Basel).* **16**, 1061 (2024).

47. Elhamnia, M., Dadashi, P. & Motlagh, G. H. Investigating competition of strong interfacial interaction and chain scission in PBAT/EVOH/GO composite by rheological measurements. *J. Reinf. Plast. Compos.* 07316844241256416 (2024).

48. Soltani, E., Motlagh, G. H., Elhamnia, M. & Dadashi, P. Highly efficient reactive compatibilization of biodegradable PBAT/EVOH blend by pMDI. *J. Appl. Polym. Sci.* e55666.

49. Wu, F. et al. Interfacial relaxation mechanisms in polymer nanocomposites through the rheological study on polymer/grafted nanoparticles. *Polymer (Guildf)*. **90**, 264–275 (2016).
50. Mofokeng, J. P. & Luyt, A. S. Morphology and thermal degradation studies of melt-mixed poly (lactic acid)(PLA)/poly (ε-caprolactone)(PCL) biodegradable polymer blend nanocomposites with TiO2 as filler. *Polym. Test.* **45**, 93–100 (2015).
51. Kalita, N. K., Bhasney, S. M., Mudenur, C., Kalamdhad, A. & Katiyar, V. End-of-life evaluation and biodegradation of Poly (lactic acid)(PLA)/Polycaprolactone (PCL)/Microcrystalline cellulose (MCC) polyblends under composting conditions. *Chemosphere* **247**, 125875 (2020).
52. Jafari, S. M. A., Khajavi, R., Goodarzi, V., Kalaee, M. R. & Khonakdar, H. A. Development of degradable poly(ethylene terephthalate)-based nanocomposites with the aid of polylactic acid and graphenic materials: Thermal, thermo-oxidative and hydrolytic degradation characteristics. *J. Appl. Polym. Sci.* **137**, (2020).
53. Jin, T. X. et al. Crystallization, mechanical performance and hydrolytic degradation of poly(butylene succinate)/graphene oxide nanocomposites obtained via in situ polymerization. *Compos. Part A Appl. Sci. Manuf.* **68**, 193–201 (2015).
54. Babaei, A., Haji Abdolrasouli, M. & Rostami, A. Polylactic acid/polycaprorlactone bionanocomposites containing zinc oxide nanoparticles: Structure, characterization and cytotoxicity assay. *J. Thermoplast. Compos. Mater.* **36**, 2998–3020 (2023).

Author contributions

1—P.D.: Wrote the main manuscript; data analysis 2—K.T.: Collected the data; performed the analysis. 3—A.B.: Reviwed the manuscript; data analysis.

Declarations

Competing interests

The authors declare no competing interests.

Data availability

The datasets used and analyzed during the current study are available from the corresponding author on reasonable request.

Additional information

Supplementary Information The online version contains supplementary material available at https://doi.org/10.1038/s41598-025-02087-8.

Correspondence and requests for materials should be addressed to A.B.

Reprints and permissions information is available at www.nature.com/reprints.

Publisher's note Springer Nature remains neutral with regard to jurisdictional claims in published maps and institutional affiliations.